

FRACTIONAL ORDER PROCESSING OF QUARTZ CRYSTAL MICROBALANCE BASED DNA BIOSENSOR SIGNALS

Anhong Zhou¹ and YangQuan Chen²

¹*Biological and Irrigation Engineering Department,
Utah State University,*

4105 Old Main Hill, Logan, UT 84322-4105, U.S.A;

²*Centre for Self-Organizing and Intelligent Systems (CSOIS)*

Electrical and Computer Engineering Department,

Utah State University,

4120 Old Main Hill, Logan, UT 84322-4120, U.S.A.

Emails: azhou@cc.usu.edu; yqchen@engineering.usu.edu

Abstract: The working principle of quartz crystal microbalance (QCM) is based on the linear relationship between the change of frequency (Δf) and the change of mass on the crystal surface, as described in Sauerbrey equation. In present work, it is interesting to observe the oscillation characteristics of Δf and resistance (R) in the early period of single strand (ssDNA) immobilization and subsequent target DNA (tDNA) hybridization. Two fractional order signal processing techniques, namely, fractional Fourier transform (FrFT) and rescaled range statistical analysis (R/S analysis), are applied to analyze the QCM signals. *Copyright © 2006 IFAC*

Keywords: Fractional order signal processing, fractional Fourier transformation (FrFT), rescaled range statistical analysis, DNA hybridization measurement, quartz crystal microbalance.

1. INTRODUCTION

The quartz crystal microbalance (QCM) is a promising tool for biosensor applications (Ward, 1991), for example, in real-time detection of DNA hybridization (Zhou, *et al.*, 2001). The Sauerbrey equation (Sauerbrey, 1959) describes a linear relationship between the frequency changes and the mass changes of the quartz crystal. The immobilization of single strand DNA (ss-DNA) on the gold coated QCM sensor surface and the hybridization of ssDNA with sequence complementary target DNA (tDNA) will be quantified by monitoring frequency differences before and after DNA immobilization and hybridization.

Synthesized oligonucleotides samples used in this experiment are specific from the heat shock protein 70 (*hsp 70*) of *Cryptosporidium parvum*, a deadly pathogenic waterborne parasite. *C. parvum* can enter waterways from non-point agricultural sources and has been recognized by the World Health Organization as a significant global health threat (WHO, 1990). Currently, there are 22 species of *C. parvum* identified (Fayer, *et al.*, 1997). However, no analytical method satisfactorily detects the *Cryptosporidium* microorganism. US Environmental Protection Agency Method 1622 (EPA 1622 web site) is time consuming and labor intensive. There is an urgent need for developing a reliable, fast and cost-effective detection method, which is a valuable goal in helping to determine the source of the pathogen in a human epidemic.

In our former research (McEwen, *et al.*, 2005), we reported two approaches (electrochemistry and SPR) to detect the hybridization of *C. parvum* DNA on gold surface by redox indicator-labeled electrochemical and label-free SPR methods. Here we lay our emphasis on the new outcomes for DNA hybridization detection based on QCM method, a real-time mass-based measurement technique. Since the QCM signals we observed contain complex dynamics, conventional signal processing techniques may not be able to indicate the right signatures. In this paper, we attempted to apply two fractional order signal processing techniques, namely, fractional Fourier transform (FrFT) (Ozaktas, *et al.*, 2001) and rescaled range statistical analysis (R/S analysis) (Geweke and Porter-Hudak, 1983, *GPH* website), to characterize the QCM signals for easy differentiation of different cases studies in this study.

2. MATERIALS AND METHODS

QCM method is performed at room temperature (20 °C) in QCA922 (AMETEK Princeton Applied Research, TN) which can measure the frequency and resistance of a quartz crystal resonator (9 MHz, AMETEK PAR) at the same time. Prior to immobilization with ss-DNA, the bare gold coated crystal surface was cleaned in Piranha solution (25% H₂O₂/75%H₂SO₄). *CAUTION: Piranha solution reacts violently with organic solvents and is a skin irritant. Extreme caution should be exercised when handling piranha solution.*

We selected an oligonucleotide length of 40-base in the *hsp 70* gene of *C. baileyi* as a control probe (labeled as “cDNA”) which has fine mismatched bases compared with the human genotype of *C. parvum* [7], and target DNA sequence (labeled as “tDNA”). Oligonucleotide sequences were obtained from SynGen, Inc. (San Carlos, CA) with 100 μM concentration when diluted in doubly distilled water (Milli-Q, MA).

t: 5'-AGAA A GG A ACTGG C GA G
AGAAATGT A T T G AT C TT C GATTT-3'
c: 5'-AGAA G GG T ACTGG T GA A
AGAAATGT T C T T AT T TT T GATTT-3'
cDNA is modified with thiol-C6 at 5' end.

3. RESULTS

3.1 QCM response to addition of water

100 μl of water was first added on bare gold coated QCM surface after it reached a stable frequency in air. Figure 1 exhibits the detailed profile of the response for the whole process. A sharp decrease of Δf and an increase of R occurred simultaneously when water was dropped on the surface at time of 0 second. The obvious oscillations of both Δf and R were observed, as designated in period II, at the early period right after the additions of samples. After

period II, as the evaporation of water from the Au surface, both Δf and R returned closely to the starting point (baseline) in air prior to any sample addition (*ca.* - 200 Hz difference). The dramatic increasing of Δf in period III in Figure 1 resulted from the most rapid evaporation of water.

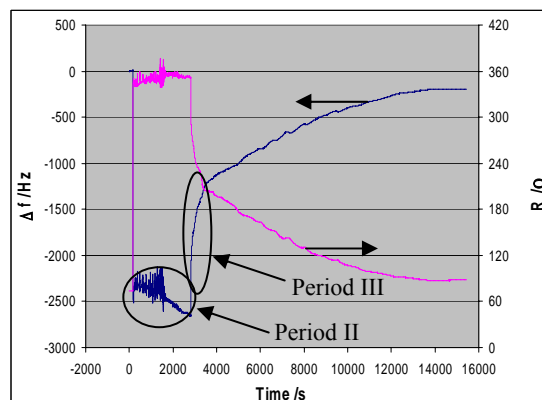


Fig. 1. The responses of Δf and R when 100 μl of water was added on gold coated QCM.

3.2 QCM response to addition of ssDNA

Figure 2 shows the Δf and R responses due to the addition of 100 μl 1 μM control probe DNA solution in distilled water on bare gold surface. Similar response curves were obtained as the case of water addition (shown in Figure 1). As the evaporation of the water, both Δf and R gradually went back, but not to the exact baseline in air because of the remaining DNA molecules immobilized on gold surface. Comparing with a starting point in air, the frequency change was -300 ~ -400Hz. Periods II and III in Figure 2 are designated as the same as in Figure 1.

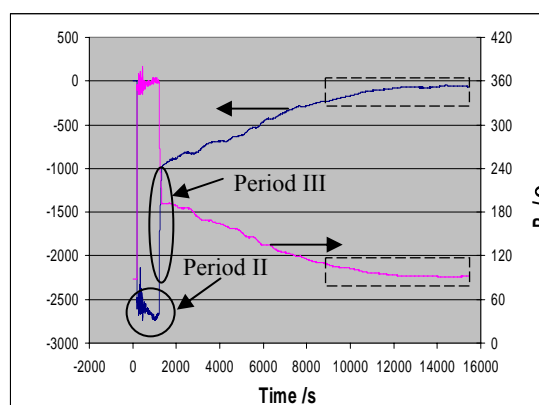


Fig. 2. The responses of Δf and R when 100 μl of 1 μM control probe DNA was added on bare Au coated with QCM. Dashed frames indicate the drifts of Δf and R in air.

3.3 QCM response to addition of tDNA

After the immobilization of ss-DNA, 100 μl of 1 μM target DNA solution in distilled water was added on the modified gold surface to allow hybridization. The changes of Δf and R during the hybridizing process are given in Figure 3. Period II is designated as the same as in Figures 1 and 2.

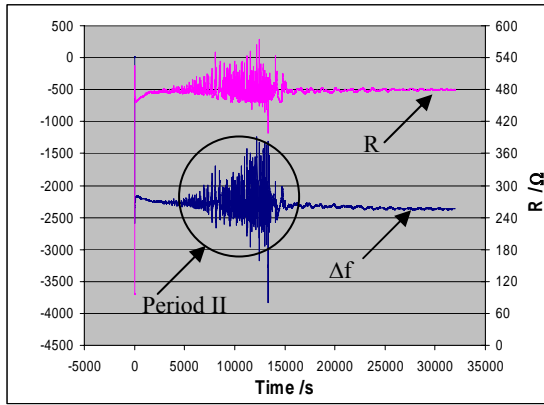


Fig. 3. The responses of Δf and R when 100 μl of 1 μM tDNA was added on control probe (100 μl of 1 μM) immobilized gold surface.

The relationships of Δf and R in periods II and III of each addition of sample solutions (water, cDNA, and tDNA) are depicted in Figure 4 (A and B). The theoretical slope of Δf and R in viscous liquids was 10 ~ 11 Hz/ (Zhou, *et al.*, 2001a), which implies the slightly larger contribution from “non-mass effect”.

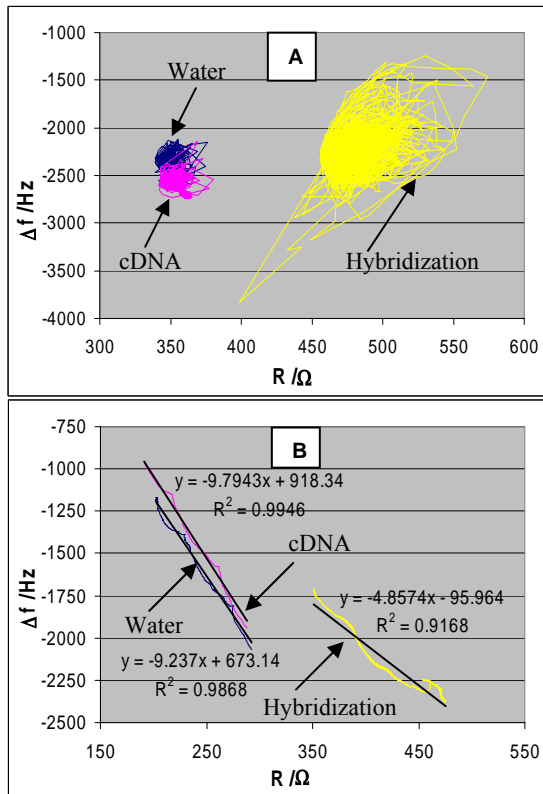


Figure 4. Relationship of Δf and R in periods II (A) and III (B) when adding water, cDNA, and tDNA, respectively.

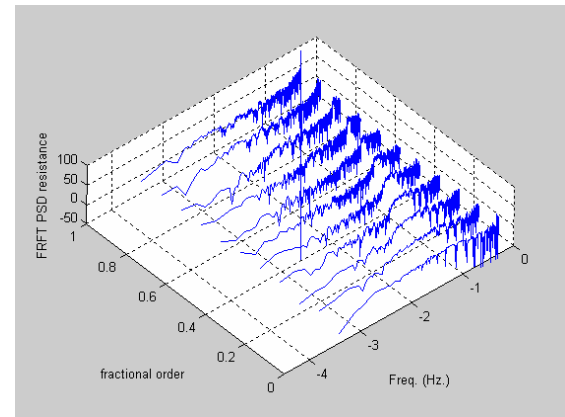
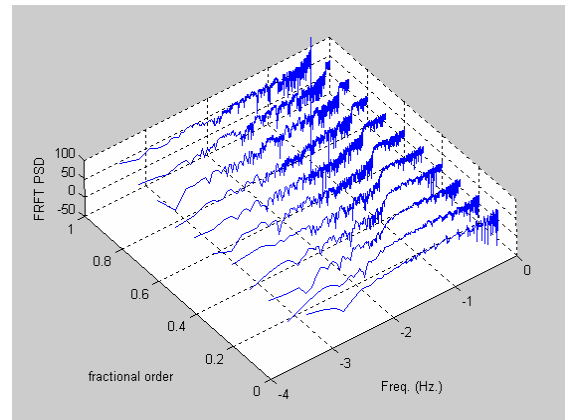
3.4 Fractional order signal processing

As we can observe from Figs. 1-3, the visual differences in the time domain seem to be clear when considering the phase transitions. However, if we only observe the signal during the liquid phase, it could be hard to give a reliable quantitative measure to tell the differences. Joint time and frequency domain characterization will be necessary since the

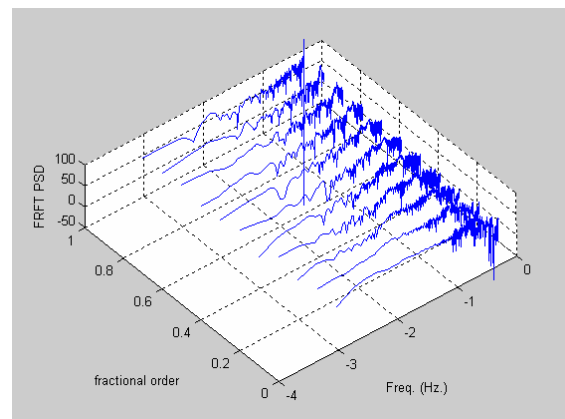
signals are highly dynamic and likely stochastic and nonstationary.

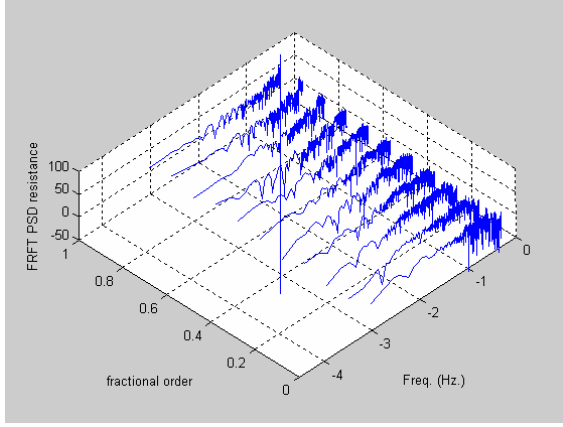
A simple exposition to discrete FrFT can follow the classical discrete Fourier transform (DFT) of a signal $f(n)$ by matrix notation $\mathbf{f}_1 = \mathbf{F}\mathbf{f}$ where \mathbf{f} is an N -by-1 column vector, \mathbf{F} is the N -by- N DFT matrix and \mathbf{f}_1 is the DFT of \mathbf{f} . Similarly, the a -th order discrete FrFT of \mathbf{f} , denoted as \mathbf{f}_a is defined as $\mathbf{f}_a = \mathbf{F}^a \mathbf{f}$ where \mathbf{F}^a is the N -by- N discrete FrFT matrix corresponding to the a -th power of the classical DFT matrix \mathbf{F} . Note that the definitions of discrete FrFT depend on the interpretations of the “power” (Ozaktas *et al.*, 2001).

Using fast discrete FrFT (Ozaktas *et al.*, 1996, Bultheel and Sulbaran, 2004), here we present the time-order representations of our QCM signals for three cases in Figure 5 below.

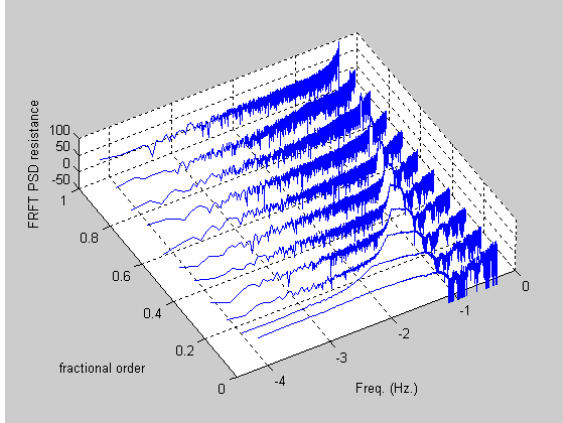
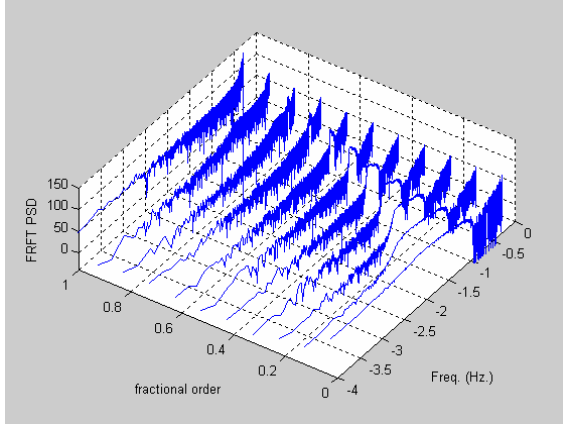


(A) Case-1: 100 μl water





(B) Case-2: 100 µl 1µM cDNA



(C) Case-3: 100 µl 1µM tDNA

Fig. 5. FrFT based time-order representation (for each case, top: frequency (f); bottom: resistance (R))

Detailed discussion on why we choose to represent our QCM signals in this way can be found in (Ozaktas, *et al.*, 2001). In simple words, just like time-frequency and time-scale signal representations, the FrFT based time-order representation constitutes an alternative way of displaying the content of a signal, with the potential to reveal features that may not be evident upon examination of its other representations. For example, in our Case-3, with target, the time-order representation displayed in Figure 5(C) is much distinguishable from Case-1 and Case-2.

Considering the possible “chaotic” behaviors in our QCM signals, we attempt to apply the so-called rescaled range statistical analysis (R/S analysis) (Bultheel and Sulbaran, 2004, Hurst 1951, *GPH* website, Geweke and Porter-Hudak, *et al.*, 1983). For a discrete time series ξ_τ , its R/S statistics are defined as follows:

$$X(t, \tau) = \sum_{u=1}^t (\xi_u - \langle \xi \rangle_\tau)$$

$$R(\tau) = \max_{1 \leq t \leq \tau} X(t, \tau) - \min_{1 \leq t \leq \tau} X(t, \tau)$$

$$S(\tau) = \left[\frac{1}{\tau} \sum_{t=1}^{\tau} (\xi_t - \langle \xi \rangle_\tau)^2 \right]^{\frac{1}{2}}$$

$$R/S(\tau) = R(\tau) / S(\tau) \quad (1)$$

where in $X(t, \tau)$, the mean over the time lag τ

$$\langle \xi \rangle_\tau = \frac{1}{\tau} \sum_{t=1}^{\tau} \xi_t$$

is removed when the expectation of ξ_τ is not 0. $R(\tau)$ is the self-adjusted range and $R/S(\tau)$ is the self-rescaled self-adjusted range. Many processes in nature are not independent random processes, but show significant long-term correlations. In this case the asymptotic scaling law is modified and $R/S(\tau)$ is asymptotically given by a power law τ^H . The corresponding exponent H is called *Hurst exponent*. *Persistent* behavior is characterized by a Hurst exponent $0.5 < H < 1$, *anti-persistence* is characterized by $0 < H < 0.5$. In general the Hurst exponent can attain values in the range $0 \leq H \leq 1$ only.

Here, we are interested to know if *Hurst exponent* for three cases are the same or not. We used the conventional Hurst-Mandelbrot method to perform the R/S analysis and to get an estimate of the Hurst exponent H . For three cases, the $\log(R/S)$ vs. $\log(n)$ plots are shown in Figure 6 where the slope is called the *Hurst exponent*.

To obtain a less noisy slope of $\log(R/S)$ vs. $\log(n)$, or H , we applied the expectation of $\log(R/S)$ and then do a linear regression. Table 1 summarizes the obtained results.

Table-1. Hurst exponents of Cases 1, 2, and 3

Cases	H (freq.)	H (resist.)
1. 100 µl water	0.52773	0.52773
2. 100 µl cDNA	0.54039	0.54039
3. 100 µl tDNA	0.51352	0.51352

We have the following observations and remarks:

- In all cases, the Hurst exponents are all greater than 0.5. This implies a *persistent* time series characterized by *long memory effects*.
- It is very interesting to see that, when the expectation of $\log(R/S)$ is used for Hurst exponent estimation, the Hurst exponents for both frequency and resistance signals are the same! This might not be surprising since both

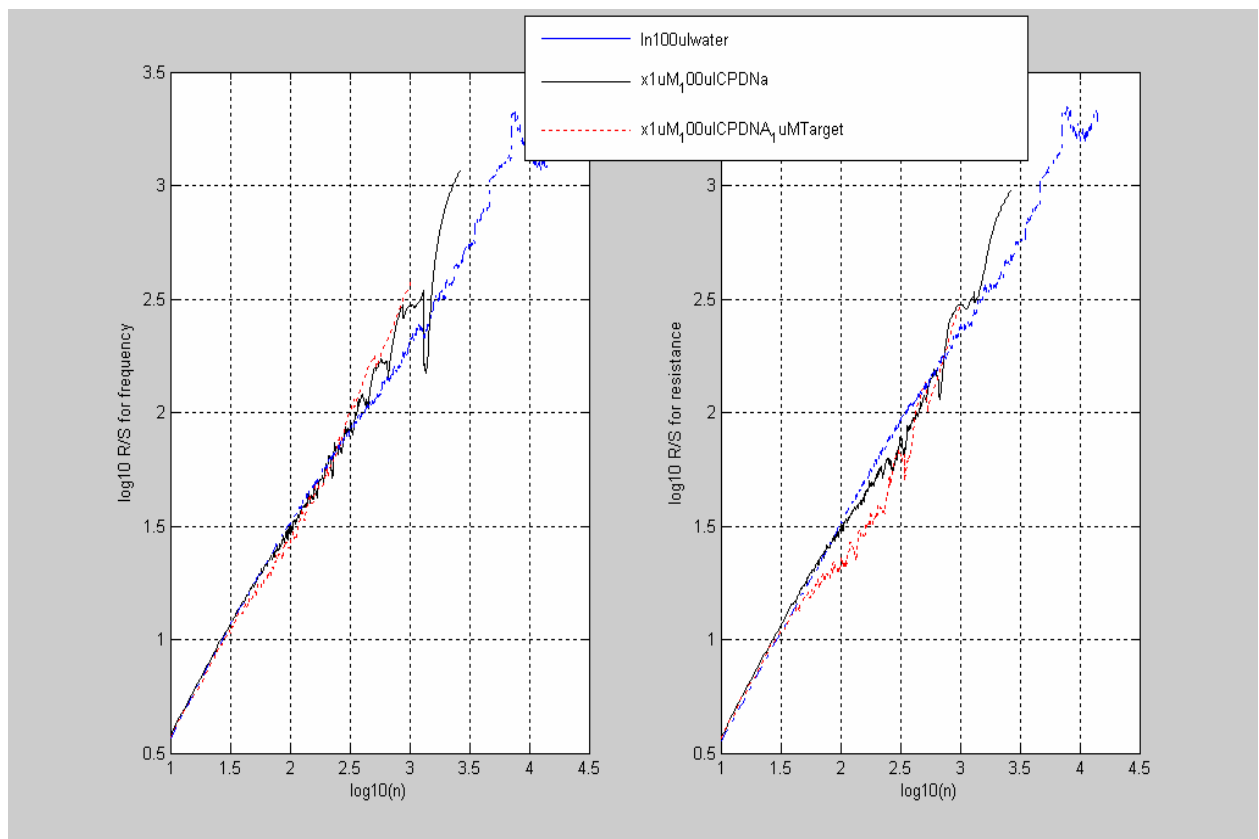


Fig. 6. Log(R/S) vs. Log(n) plot for Cases 1, 2, and 3.

signals are affected by the same evaporation dynamics.

- With the target, the Hurst exponent for Case-3 is even smaller than that of the Case-1. This deserves a good explanation.

The Hurst exponents obtained can be served as a quantitative indicator to differentiate different cases such as different concentrations, difference biological materials, different bioreactions, and etc.

4. CONCLUSIONS

The frequency and resistance oscillation curves of QCM in the additions of water, cDNA immobilization, and tDNA hybridization were recorded. The water evaporation processes in these three cases implies the “non-mass effect” contribution to the frequency changes. We have also attempted two fractional order signal processing techniques, namely, fractional order Fourier transformation and rescaled range statistical analysis for Hurst exponent estimation, and the preliminary results are encouraging towards quantifying biological processes in general and biosensing process in particular.

ACKNOWLEDGEMENT

This work was supported in part by the USU SDL “Skunkworks” Research Initiative Grant Program.

REFERENCES

Bultheel, A. and H.M. Sulbaran (2004). Computation of the Fractional Fourier Transform” *Applied and Computational Harmonic Analysis*, *Appl. Comput. Harmonic Anal.*, **16**, 182-202.

EPA 1622, *Cryptosporidium* in Water by Filtration/IMS/FA
<http://www.epa.gov/nerlcwww/1622ap01.pdf>

Fayer R, C.A. Spear, and J. P. Dubey (1997). The general biology of *Cryptosporidium*. In: *Cryptosporidium and cryptosporidiosis*, (R. Fayer (Ed.), p. 1-41, CRC Press, Boca Raton, Fla.

Geweke, J. and S. Porter-Hudak (1983), The Estimation and Application of Long Memory Time Series Models, *J. Time Series Anal.*, **4**, 221-238,

GPH: MATLAB module to calculate Geweke-Porter-Hudak long memory statistic,
<http://ideas.repec.org/c/boc/bocode/t850805.html>

Hurst H.E. (1951), Long-term storage capacity of reservoirs, *Trans. Am. Soc. Civil Eng.*, **116**, 770-790.

McEwen, G., M. Grover and A. Zhou (2005), Electrochemical and surface plasmon resonance detection of pathogenic DNA, *1st Annual Mountain Biomedical Engineering Conference*, Sept 16-17, Snowbird, Utah.

Ozaktas, H.M., M.A. Kutay and G. Bozdagi (1996). Digital computation of the fractional Fourier transform, *IEEE Trans. Sig. Proc.*, **44**, 2141—2150.

Ozaktas, H.M., Z. Zalevsky and M. A. Kutay (2001). The Fractional Fourier Transform with Applications in Optics and Signal Processing. In: *Series in Pure and Applied Optics. XVIII*, John Wiley & Sons.

Sauerbrey G. (1959). Verwendung von Schwingquarzen zur Wägung dünner Schichten und zur Mikrowägung *Z Phys.*, **155**, 206-222.

WHO Reports Decry Neglect of World Health Problems (1990), *ASM News*, 56, 358.

Ward, M. D. (1995). Principles and Applications of the Electrochemical Quartz Crystal Microbalance. In: *Monographs in Electroanalytical Chemistry and Electrochemistry: Physical Electrochemistry, Principles, Methods, and Applications*, (I. Rubinstein. (Ed.)), Marcel Dekker, New York.

Zhou A, Q. Xie and S. Yao (2001a). A defect coefficient – new insight into the responses of piezoelectric quartz crystal in gaseous and liquid phase. *Sens. Actuators A*, **88**, 227-233.

Zhou X.C., L.Q. Huang and S.F. Li (2001b). Microgravimetric DNA sensor based on quartz crystal microbalance: comparison of oligonucleotide immobilization methods and the application in genetic diagnosis. *Biosens Bioelectron.*, **16**, 85-95.